rock glaciers or thawing of frozen ground[24]. In general, field campaigns should be targeted towards critical locations, e.g. where lakes are dammed in permafrost terrain, and ideally areas where there is good access in view of long-term monitoring and repeat visits.

The Kullu pilot study has provided some preliminary understanding of the possible extent and relevance of permafrost in this region. Scientific partnerships established within this study now provide a sound basis for formulating further measurement and monitoring projects that may extend across the wider Himalayan area in future.

1. Mayewski, P. A. and Jeschke, P. A., An active rock glacier, Wavbal Pass, Jammu and Kashmir Himalaya, India. *J. Glaciol.*, 1981, **27**(95), 201–202.
2. Owen, L. A. and England, J., Observations on rock glaciers in the Himalayas and Karakoram Mountains of northern Pakistan and India. *Geomorphology*, 1998, **26**, 199–213.
3. Schmid, M.-O., Baral, P., Gruber, S., Shahi, S., Shrestha, T., Stumm, D. and Wester, P., Assessment of permafrost distribution maps in the Hindu Kush Himalayan region using rock glaciers mapped in Google Earth. *Cryosphere*, 2015, **9**, 2089–2099.
4. van Everdingen, R. (ed.), *Multi-Language Glossary of Permafrost and Related Ground-Ice Terms*, National Snow and Ice Data Center, Boulder, CO, USA, 1998.
5. Vaughan, D. G. *et al.*, *Observations: Cryosphere*, in *Climate Change 2013: The Physical Science Basis. Contribution of Working Group I to the Fifth Assessment Report of the Intergovernmental Panel on Climate Change* (eds Stocker, T. F. *et al.*), Cambridge University Press, Cambridge, United Kingdom, 2013, pp. 317–382.
6. Harris, C., Climate change, mountain permafrost degradation and geotechnical hazard. In *Global Change and Mountain Regions. An Overview of Current Knowledge* (eds Huber, U. M., Bugmann, H. K. M. and Reasoner, M. A.), Springer, Dordrecht, 2005, pp. 215–224.
7. Yang, M., Nelson, F. E., Shiklomanov, N. I., Guo, D. and Wan, G., Permafrost degradation and its environmental effects on the Tibetan Plateau: a review of recent research. *Earth-Sci. Rev.*, 2010, **103**, 31–44.
8. Sorg, A., Bolch, T., Stoffel, M., Solomina, O. and Beniston, M., Climate change impacts on glaciers and runoff in Tien Shan (Central Asia). *Nature Climate Change*, 2012, **2**, 725–731.
9. Gruber, S., Derivation and analysis of a high-resolution estimate of global permafrost zonation. *Cryosphere*, 2012, **6**, 221–233.
10. Kulkarni, A. V. and Karyakarte, Y., Observed changes in Himalayan glaciers. *Curr. Sci.*, 2014, **106**(2), 237–244.
11. Etzelmüller, B. *et al.*, Mapping and modelling the occurrence and distribution of mountain permafrost. *Norw. J. Geogra.*, 2001, **55**, 186–194.
12. Hoelzle, M., Permafrost occurrence from BTS measurements and climate parameters in the Eastern Swiss Alps. *Permafrost Periglacial Process.*, 1992, **3**, 143–147.
13. Imhof, M., Modelling and verification of the permafrost distribution in the Bernese Alps, Western Switzerland. *Permafrost Periglacial Process.*, 1996, **7**, 267–280.
14. Fiddes, J. and Gruber, S., TopoSUB: A tool for efficient large area numerical modelling in complex topography at sub-grid scales. *Geosci. Model Develop.*, 2012, **5**, 1245–1257.
15. Fiddes, J. and Gruber, S., TopoSCALE v.1.0: downscaling gridded climate data in complex terrain. *Geosci. Model Develop.*, 2014, **7**, 387–405.
16. Haeberli, W. *et al.*, Permafrost creep and rock glacier dynamics. *Permafrost Periglacial Process.*, 2006, **17**, 189–214.
17. Bhutiyani, M. R., Kale, V. S. and Pawar, N. J., Long-term trends in maximum, minimum and mean annual air temperatures across the Northwestern Himalaya during the twentieth century. *Climatic Change*, 2007, **85**, 159–177.
18. Fukui, K., Fujii, Y., Ageta, Y. and Asahi, K., Changes in the lower limit of mountain permafrost between 1973 and 2004 in the Khumbu Himal, the Nepal Himalayas. *Global Planet. Change*, 2007, **55**, 251–256.
19. Noetzli, J. and Gruber, S., Transient thermal effects in Alpine permafrost. *Cryosphere*, 2009, **3**, 85–99.
20. Ives, J. D., Shrestha, R. B. and Mool, P. K., Formation of glacial lakes in the Hindu Kush-Himalayas and GLOF risk assessment, ICIMOD, Kathmandu, 2010.
21. Worni, R., Huggel, C. and Stoffel, M., Glacier lakes in the Indian Himalayas – from an area-wide glacial lake inventory to on-site and modeling based risk assessment of critical glacial lakes. *Sci. Total Environ.*, 2013, **468–469**, s71–s84.
22. Gubler, S., Fiddes, J., Keller, M. and Gruber, S., Scale-dependent measurement and analysis of ground surface temperature variability in alpine terrain. *Cryosphere*, 2011, **5**, 431–443.
23. Hauck, C., New concepts in geophysical surveying and data interpretation for permafrost terrain. *Permafrost Periglacial Process.*, 2013, **24**, 131–137.
24. Kääb, A., Remote sensing of permafrost-related problems and hazards. *Permafrost Periglacial Process.*, 2008, **19**, 107–136.

ACKNOWLEDGEMENTS. This study is being supported by and implemented within IHCAP (www.ihcap.in), a project under the Global Programme Climate Change of the Swiss Agency for Development and Cooperation in cooperation with the Department of Science and Technology, Government of India, and with support from the Government of Himachal Pradesh.

Received 3 September 2015; revised accepted 25 January 2016

doi: 10.18520/cs/v111/i3/550-553

Identification of potential glacial lake sites and mapping maximum extent of existing glacier lakes in Drang Drung and Samudra Tapu glaciers, Indian Himalaya

U. S. Maanya, Anil V. Kulkarni*, Alok Tiwari, Enakshi Dasgupta Bhar and J. Srinivasan

Divecha Centre for Climate Change, Indian Institute of Science, Bengaluru 560 012, India

The Himalayan glaciers feed major Asian river systems sustaining the lives of more than 800 million people. Though the rates of retreat of individual glaciers are uncertain, on the whole the Himalayan

*For correspondence. (e-mail: anilkulkarni@caos.iisc.ernet.in)

glaciers have been losing mass at an increasing rate over the past few decades. With the changing climate, glaciers will continue to shrink and the rates of retreat may increase even further. This may lead to the formation of moraine dammed glacial lakes, which can cause outburst floods upon failure of the dam, catastrophic to human life and infrastructure downstream. Therefore, identification of potential lake sites and predicting the expansion of existing lakes are crucial for timely monitoring and mitigation of these hazards. In the present study, glacier surface velocity and slope are used to calculate ice thickness, by applying a basic parallel flow model, subsequently outlining the bed topography and locating potential lake sites in over-deepenings in the bedrock. Comparison of the modelled and measured ice thickness values on Chhota Shigri glacier suggests a model uncertainty of ±15%. The model is further applied to Samudra Tapu and Drang Drung glaciers using satellite data between the years 1999 and 2001, where eight potential lake sites were identified with mean depths varying between 33 ± 5 and 93 ± 14 m, of which three sites have a volume greater than 0.01 km^3. The analysis predicts an over-deepening near the snout of Samudra Tapu, in close proximity to an existing moraine dammed lake. A portion of the predicted site has already evolved into a lake between the years 2000 and 2015, which upon further deglaciation could lead to an expansion of the existing lake by an area of 14 ± 2 ha. This observation further validates the model prediction of lake expansion. The present study demonstrates the utility of the model to predict maximum expansion of the existing lakes and possible formation of new lakes due to glacier retreat. Systematic application of this technique can provide information crucial to policy makers and planners dealing with the security of people living in the mountains.

Keywords: Bed topography, glacial lakes, ice thickness, remote sensing.

IN the recent past many glaciers around the world, including those in the Himalaya have been experiencing retreat[1]. Though there is uncertainty in the rates of retreat of individual glaciers, on the whole the Himalayan glaciers have been losing mass at an increasing rate over the past few decades[2,3]. With the changing climate they are expected to lose more mass and the rates of retreat may increase further[4]. Unabated retreat of glaciers can lead to the formation of glacial lakes that are typically bound by loose soil and debris, which can cause glacier lake outburst floods (GLOFs) upon failure of a dam and cause serious havoc downstream in a matter of a few hours[5].

The earliest GLOF events in the Indian Himalaya have been reported from Shyok glaciers, Jammu and Kashmir, as early as 1835 (ref. 6). Floods from outburst of moraine dammed lakes at Shaune Garang glacier, Himachal Pradesh were reported in 1981 and 1988 (ref. 7). In 2013, failure of the moraine dam of Chorabari lake led to flash floods which devastated Kedarnath town[8]. In order to predict such GLOF events, numerous inventories on glacial lakes have been carried out in the Indian Himalaya. One of these inventories suggests the presence of 251 glacial lakes (>0.01 sq. km) of which 105 present GLOF risk, 12 of them being critical[9–11]. However, there have been no studies to predict the maximum possible expansion of the existing lakes, which is crucial because lake volume determines the peak discharge and hence the severity of GLOF[12]. Thus identification of potential lake sites and mapping the maximum possible extent of the existing lakes are crucial to enable timely monitoring and to mitigate possible hazards.

Glaciers modify the landscape of the underlying bedrock by erosion as they move. Knowledge of this sub-glacial topography is imperative to identify bed over-deepenings, which could be potential sites for the formation of lakes as the glaciers retreat[13]. This is accomplished in the present study by applying a basic model of glacier flow parallel to the bed, to relate ice thickness along the central flowline with surface slope and velocity[14]. Ice thickness is then interpolated to the glacier boundary and subtracted from the surface elevations to obtain the bed topography. The model is validated on Chhota Shigri and is then applied to Drang Drung and Samudra Tapu in the Western Himalaya.

We have selected Chhota Shigri, Drang Drung and Samudra Tapu glaciers in the Indian Himalaya for this study. We applied the methodology to Chhota Shigri, one of the few well-studied glaciers in the Indian Himalaya for which GPR measurements are available[15]. The results obtained for Chhota Shigri were used to validate the methodology, which was thereafter applied to Drang Drung and Samudra Tapu. Table 1 provides the salient parameters of the glaciers.

To estimate glacier surface velocities, we have used Landsat data of 30 m spatial resolution (http://earthexplorer.usgs.gov/). Table 2 provides the image specifications. Glacier boundaries available from the RGI repository were used in this study (http://www.glims.org/RGI/). ASTER DEMs were used for Chhota Shigri and Samudra Tapu, while SRTM DEM was used for Drang Drung (http://earthexplorer.usgs.gov/).

Satellite images were cross-correlated to estimate glacier surface velocities and subsequently the ice thickness distribution was calculated using basic parallel flow models of glacier flow. Bed topography was then estimated by subtracting ice thickness from the surface elevations and over-deepenings in the bed were identified.

Table 1. Parameters of the glaciers selected for the present study

Glacier	Elevation (m amsl)	Area (sq. km)	Length (km)
Chhota Shigri	~4050–6200	16 ± 1	9
Drang Drung	~4100–6250	62 ± 5	23
Samudra Tapu	~4150–6150	65 ± 5	16.5

Table 2. Specifications of the satellite images used in the study

Glacier	Scene ID	Sensor	Date
Chhota Shigri	l8_11_August_2014_p147_r38	OLI	11 August 2014
	l8_15_September_p147_r38	OLI	15 September 2015
Drang Drung	LE71480371999229AGS00	ETM+	17 August 1999
	LE71480372000296SGS00	ETM+	22 October 2000
Samudra Tapu	LE71470372001179SGS00	ETM+	28 June 2001
	LE71470372002214SGS00	ETM+	2 August 2002

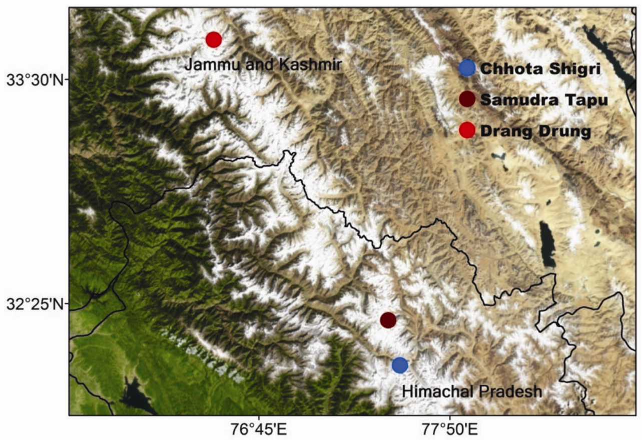

Figure 1. Landsat ETM+ image showing the location of Chhota Shigri, Samudra Tapu and Drang Drung glaicers. Chhota Shigri and Samudra Tapu are located in Himachal Pradesh, while Drang Drung is in Jammu and Kashmir, India.

Glacier surface velocities were estimated by sub-pixel correlation of multi-temporal satellite images with the help of COSI-Corr, a software module integrated in ENVI (freely available from http://www.tectonics.caltech.edu/slip_history/spot_coseis/index.html). Satellite images were co-registered to obtain the horizontal and vertical displacements along with the signal-to-noise ratio (SNR) images. The SNR image quantifies the correlation accuracy; all pixels with SNR value less than 0.9 are considered erroneous and hence discarded. Further, velocity estimates in regions with debris or snow cover could be erroneous and can be filtered by setting a threshold. In the present analysis, a threshold was applied for Chhota Shigri as velocity measurements were available from the literature, while for the other glaciers we did not apply any threshold due to non-availability of data. After removal of the erroneous pixels, the two-norm of the horizontal and vertical displacement images was calculated to find the resultant displacement magnitude. The difference in the time of acquisition between the two images, roughly a year in our study, was then used to compute the surface velocity values.

The ice thickness distribution is determined using the equation

$$H = \sqrt[4]{\frac{1.5U_s}{Af^3(\rho g \sin\alpha)^3}},$$

where H is the ice thickness (m), ρ the ice density which is assigned a constant value of 900 kg m^{-3} (ref. 16), g the acceleration due to gravity which is 9.8 m s^{-2}, f the shape factor, with a constant value of 0.8 (ref. 17), A the creep parameter, assigned a value of 2.4×10^{-24} Pa^{-3} s^{-1} (ref. 13), U_s the surface velocities, and α is the slope angle estimated over 100 m elevation contours such that the slope is averaged over a distance of at least one magnitude greater than the local ice thickness[13].

The above ice thickness distribution equation has been derived from the equation for laminar flow of glacier ice and basal shear stress[13,14]. Ice thickness was calculated along the central flow line for each sectional area between successive 100 m contours. To get the spatial distribution of ice thickness interpolation was performed using TopoToRaster, a discretized thin plate spline interpolation technique modified to ensure drainage connectivity[18], that has been previously used for interpolation of ice thickness[19,20]. A complete description of the algorithm has been done by Gantayat 2016 (pers. commun.).

The ice thickness distribution was subtracted from the surface topography to obtain the bedrock topography. Subsequently, the over-deepenings were identified by filling the sinks in the bed with the ArcGIS hydrology tool 'fill'. The difference between the filled bed and the original bed topography was to quantify the area and volume of the over-deepenings. The maximum and mean over-deepining depths were estimated at a 20 m contour interval, considering only those over-deepenings where their mean depth was greater than the model uncertainty. Eventually the volumes were computed using the depth–area relationship.

The uncertainties in the ice thickness values of Chhota Shigri were estimated using the equation

$$\frac{dH}{H} = \sqrt{\left(\frac{1}{4}\frac{dU_s}{U_s}\right)^2 + \left(\frac{3}{4}\frac{df}{f}^2\right) + \left(\frac{3}{4}\frac{d\rho}{\rho}\right)^2 + \left(\frac{3}{4}\frac{d\sin(\alpha)}{\sin(\alpha)}\right)^2}.$$

(i) Uncertainty in estimation of surface velocities, U_s: There are three sources of uncertainty while estimating surface velocities from satellite images – orthorectification errors, misregistration between the images and limitations of the correlation technique. The accuracy of image co-registration for Landsat ETM+ images has been

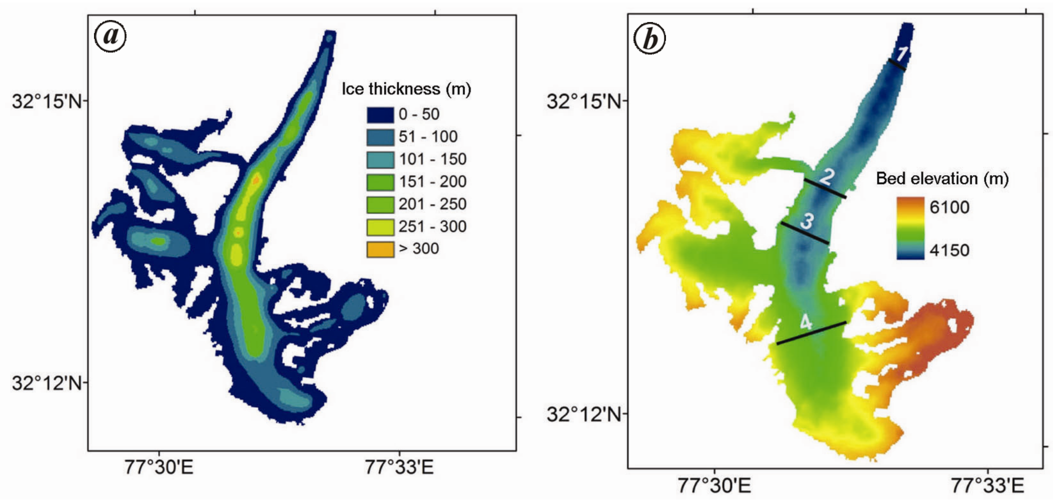

Figure 2. ***a***, Maximum ice thickness of ~300 m observed for Chhota Shigri. ***b***, The four profiles shown are used to compare the modelled bed profiles with the GPR bed profiles.

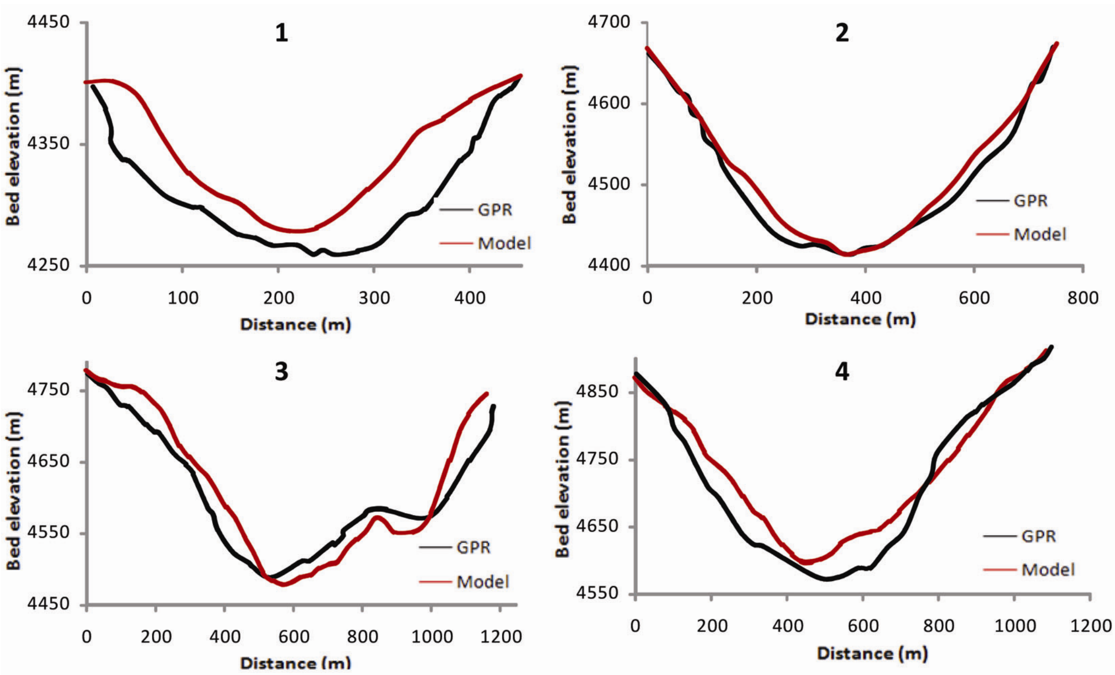

Figure 3. Measured bed profiles for Chhota Shigri reproduced fairly well by the model.

determined as 5 m (ref. 21). Accuracy of the correlation technique in COSI-Corr is of the order of ~1/20th of a pixel or 1.5 m (ref. 22). The combined accuracy is 5.2 m.

(ii) Uncertainty in calculating slope angle, α: Uncertainties arise while calculating $\sin(\alpha)$ because of vertical inaccuracies in the digital elevation model (DEM). Unfortunately, there are no ground survey data for validation of the DEM. However, in the Bhutan Himalaya vertical inaccuracies (rms) of 11.0 m for ASTER and 11.3 m for SRTM were observed[23]. Due to the similarity in topography, we have considered similar values of vertical accuracy and estimate an uncertainty of ±0.087% or ±8.7% in the $\sin(\alpha)$ values.

(iii) Uncertainty in the value of shape factor, f: shape factor represents the influence of side drag on the glacier stress balance along the central flow line, and its value varies according to the glacier width[24]. In previous studies, a constant value of 0.8 was assumed throughout the glacier, while in one study values of 0.7 and 0.9 were used for the ablation and accumulation region respectively[17,19]. Considering this range of values between 0.7 and 0.9, we get a relative uncertainty of ±0.125% or ±12.5% in the present analysis. The uncertainty can be reduced by calibrating the shape factor wherever ice thickness measurements are available.

(iv) Uncertainty in the ice density, ρ: The density of glacier ice is assumed to be 900 kg m^{-3} in the present study, like some other similar studies[16,19]. But glacier ice density varies depending on depth, which affects the pressure on the ice, and also on the proportion of air bubbles present in the ice[13]. The uncertainty is calculated considering the typical variation in ice density from 830 to 923 (ref. 10). This leads to an uncertainty of ±0.1% or ±10%.

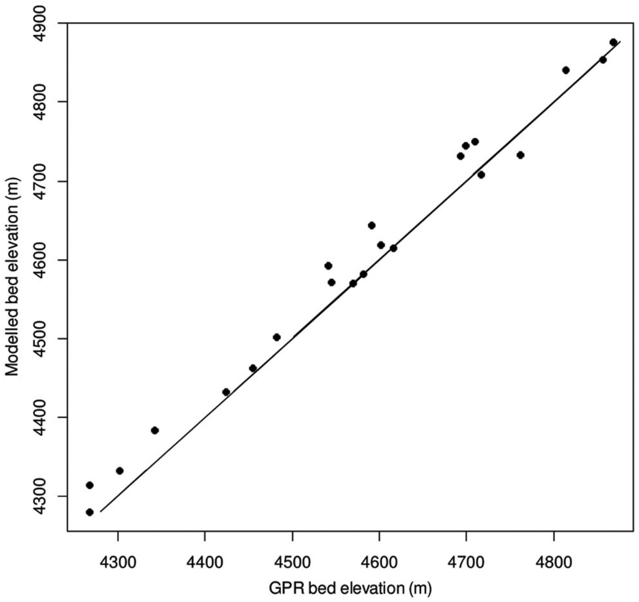

Figure 4. Scatterplot showing good correlation between GPR and modelled bed elevation values of Chhota Shigri (r = 0.99).

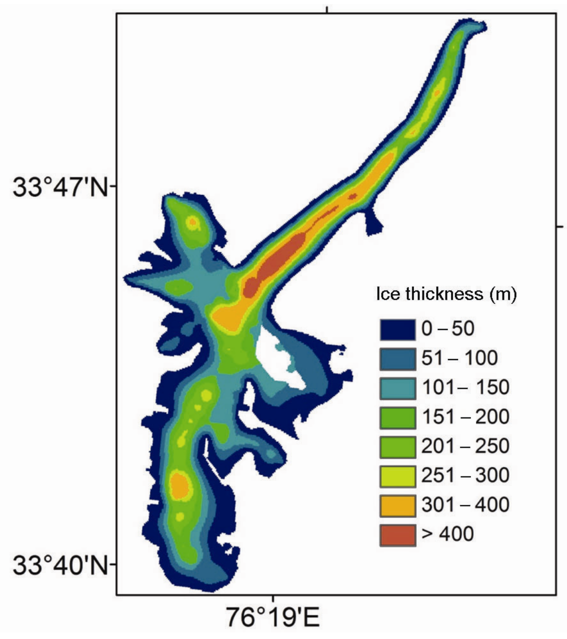

Figure 5. Ice thickness of Drang Drung varying from ~100 m at the snout to >400 m in the mid-ablation region.

The combined uncertainty is ±14.6%. Also, interpolation introduces further uncertainty in the ice thickness values and is quantified using the standard error generated by the interpolation algorithm, ±0.065% or ±6.5% in the present analysis[18]. The overall ice thickness uncertainty is therefore ~±15%.

The ice thickness and bed topography results of Chhota Shigri were compared with the GPR measurements[15]. Maximum ice thickness and bed topography measurements are available for four cross-sections along the glacier (Figure 2 *b*). The results were not validated for the fifth cross-section as it is in the confluence zone, where ice thickness estimates could be erroneous because the flow in confluence regions is not parallel to the bed and

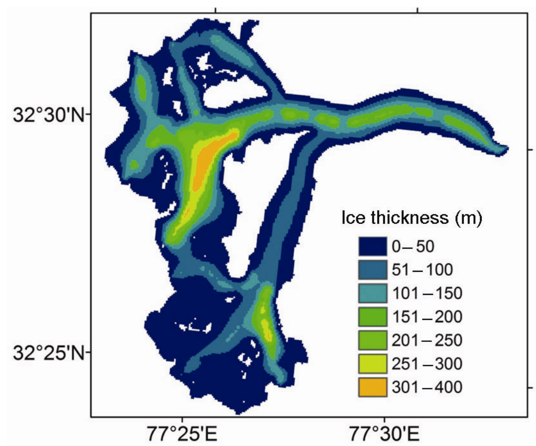

Figure 6. Maximum ice thickness of ~350 m observed for Samudra Tapu.

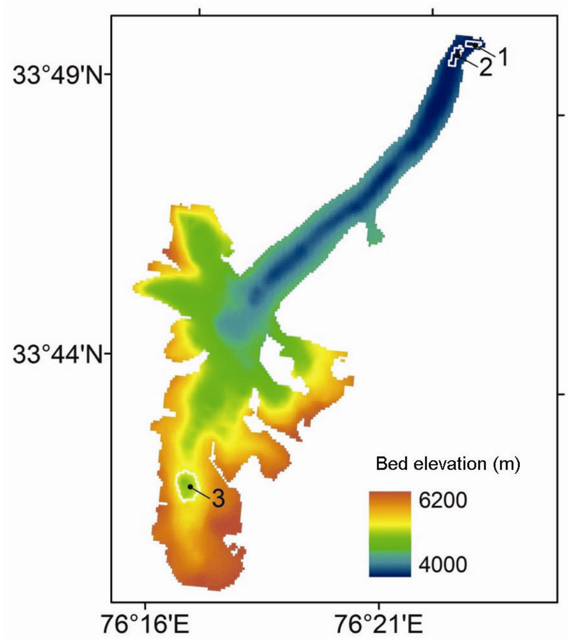

Figure 7. Three potential lake sites identified for Drang Drung with mean depth varying between 40 and 75 m.

the flow assumptions may not hold. There is a general agreement within the model uncertainty range of ±15% for maximum ice thickness as shown in Table 3, except cross-section 1. This could be due to the difference in the time period between the measured (2005) and modeled (2015) values, and possible melt during this period owing to its proximity to the snout. We were also able to reproduce the bed profiles fairly well (Figure 3). We observed a correlation coefficient of 0.99 between the modelled and GPR bed profiles, although our calculated estimates tend to be higher (Figure 4).

The ice thickness distribution of Drang Drung is fairly uniform, with a depth of ~100 m at the snout and 50–400 m in the accumulation region (Figure 5). Drang Drung has two tributaries which meet the main trunk in the mid-ablation region. The right and left tributaries have ice thickness values in the range 50–150 and 50–300 m respectively, while values as high as 400–500 m are modelled in the mid-ablation region of the main trunk. However, these high estimates may be erroneous, as they are observed in the confluence region where the parallel flow assumption may not be valid. In the case of Samudra Tapu, the ice thickness is observed to be ~150 m in the snout area. The depth increases to 150–250 m in the mid-ablation region; however, maximum ice thickness is estimated to be ~350 m in the wider accumulation region (Figure 6).

Table 3. Error in maximum ice thickness estimates for Chhota Shigri

	Ice thickness		
Cross-section	Measured (m)	Modelled (m)	Error (%)
1	124 ± 15	92 ± 14	25
2	240 ± 15	233 ± 35	3
3	245 ± 15	265 ± 40	8
4	270 ± 15	230 ± 35	15

Table 4. Statistics of potential lake sites for Drang Drung

Lake	Maximum depth (m)	Area (ha)	Volume (10^6 m^3)
1	55 ± 8	9.2	3.8 ± 0.5
2	94 ± 12	17.2	6.7 ± 1.2
3	152 ± 23	69.4	46.8 ± 7

Table 5. Statistics of potential lake sites for Samudra Tapu

Lake	Maximum depth (m)	Area (ha)	Volume (10^6 m^3)
1	80 ± 12	44	9.7 ± 2
2	57 ± 9	24	5.45 ± 0.5
3	55 ± 8	49	7.2 ± 0.5
4	43 ± 6	5	1.7 ± 0.3
5	200 ± 30	89	51.2 ± 2.5

From the ice thickness distribution, bed topography of Drang Drung and Samudra Tapu were estimated. We have identified eight potential lake sites, having volume $>10^6$ m^3, at the bottom of the glaciers. Three sites were

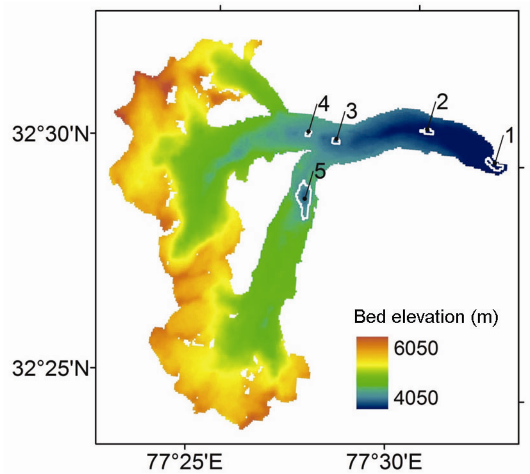

Figure 8. Five potential lake sites identified for Samudra Tapu with mean depth varying between 35 and 95 m.

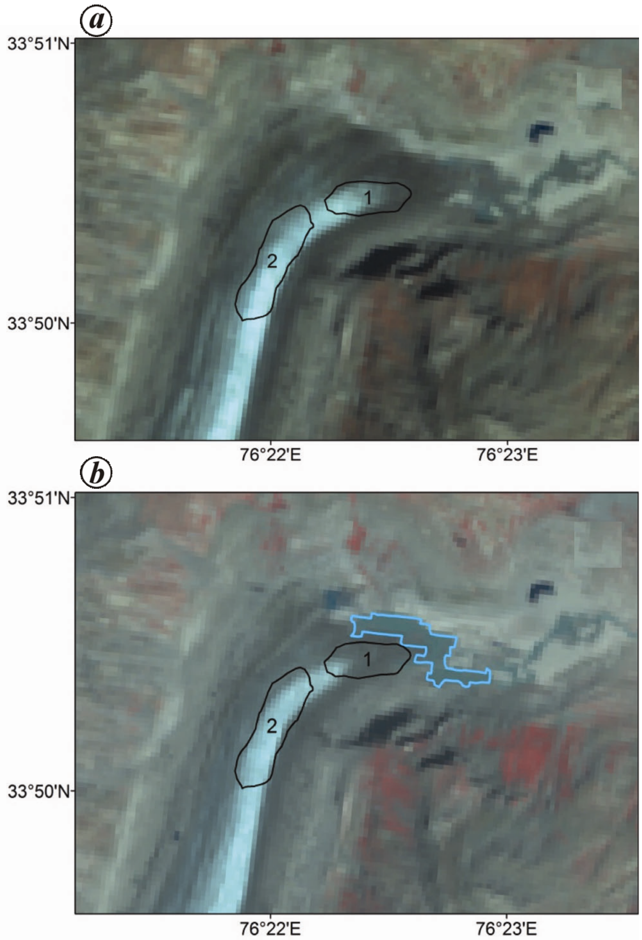

Figure 9. ***a***, Lakes predicted near the snout of Drang Drang for the year 2000. ***b***, Formation of a shallow lake near site 1 as seen in 2014.

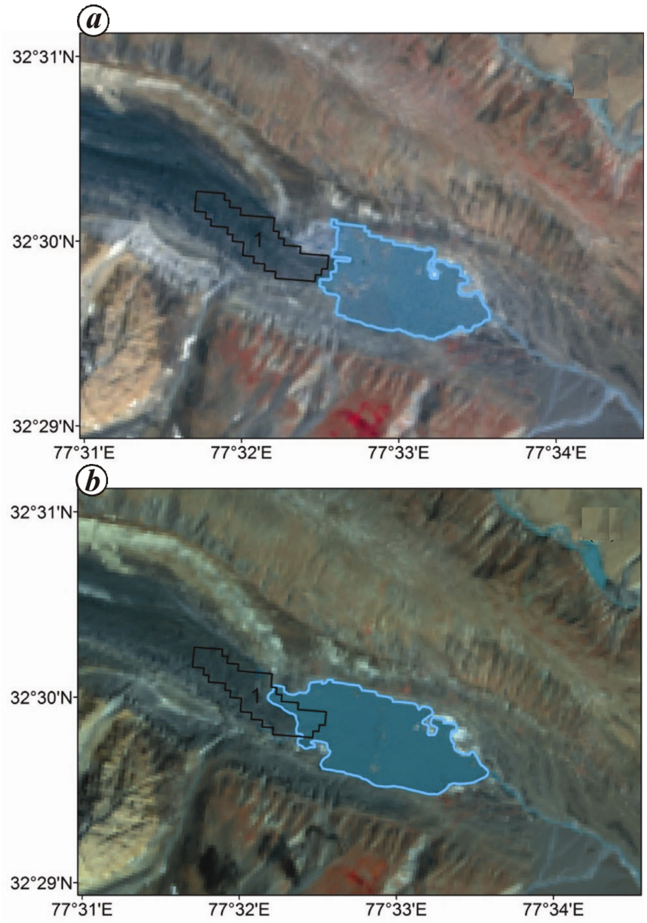

Figure 10. ***a***, Snout position of Samudra Tapu and an existing moraine dammed lake as seen in 2002, along with the predicted lake site. ***b***, As of 2015, the lake has expanded and it also covers a part of site 1.

identified for Drang Drung (Figure 7), with mean depth varying from 55 to 152 m (Table 4). Prolonged retreat could lead to the formation of lakes at sites 1 and 2 in the near future due to their proximity to the snout. For Samudra Tapu five potential lake sites were identified, with volume as high as 0.017 km^3. The maximum depths of the over-deepenings vary from 45 to 200 m and the area from 5 ha to 89 ha (Table 5). Site 1 is in close proximity to the snout (Figure 8) with a maximum depth of ~80 m and volume of 0.009 km^3.

In this study we have used surface velocity and slope, along with basal shear stress and laminar flow equations, to estimate glacier depth and bottom topography. Over-deepenings in the bedrock can help in the identification and mapping of potential lake sites. We have identified 12 potential sites for lake formation on Drang Drung and Samudra Tapu, with one site each near their respective snouts (Figures 7 and 8). As this study was carried out using 2001/2002 and 1999/2000 satellite images for Samudra Tapu and Drang Drung respectively, the latest available images were analysed to assess the evolution of the sites near the snouts, providing us an opportunity to validate our results. Formation of a shallow lake near the snout of Drang Drung is observed on the satellite imagery of 2014, which was not seen for the year 2000 (Figure 9). Deglaciation of site 1 could lead to further expansion of the existing lake by ~9.2 ha. In the case of Samudra Tapu, a moraine-dammed lake already exists near the snout[25]. Our analysis suggests that a portion of site 1 is already a part of this lake (Figure 10). As of 2015, the area of the lake was ~138 ha and further retreat could therefore lead to an increase in its area by ~14 ha and volume by ~0.013 km^3.

The present study demonstrates the utility of remote sensing data, such as satellite images, glacier boundary and DEM, in estimating glacier depth and bottom topography. This provides an effective means for predicting formation of new glacial lakes as well as expansion of existing ones.

1. Zemp, M. *et al.*, Historically unprecedented global glacier decline in the early 21st century. *J. Glaciol.*, 2015, **61**, 745–761.
2. Bolch, T. *et al.*, The state and fate of Himalayan glaciers. *Science*, 2012, **336**, 310–314.
3. Kulkarni, A. V. and Karyakarte, Y., Observed changes in Himalayan glaciers. *Curr. Sci.*, 2014, **106**(2), 237–244.
4. Chaturvedi, R. K., Kulkarni, A. V., Karyakarte, Y., Joshi, J. and Bala, G., Glacial mass balance changes in the Karakoram and Himalaya based on CMIP5 multi-model climate projections. *Climatic Change*, 2014, **123**(2), 315–328.
5. Richardson, S. D. and Reynolds, J. M., An overview of glacial hazards in the Himalayas. *Quaternary Int.*, 2000, **65/66**, 31–47.
6. Mason, K., Indus floods and Shyok glaciers. *Himalayan J.*, 1929, **1**, 10–29.
7. Sangewar, C. V., Srivastava, D. and Singh, R. K., Reservoir within the Shaune Garang glacier, district Kinnaur, Himachal Pradesh. In Proceedings of the Symposium on Snow, Ice and Glaciers: A Himalayan Perspective. Geological Survey of India, Abstr., 1999, pp. 39–40.
8. Dhobal, D. P., Gupta, A. K., Mehta, M. and Khandelwal, D. D., Kedarnath disaster: facts and plausible causes. *Curr. Sci.*, 2013, **105**(2), 171–174.
9. Worni, R., Huggel, C. and Stoffel, M., Glacial lakes in the Indian Himalayas – from an area wide glacial lake inventory to on-site and modeling based risk assessment of critical glacial lakes. *Sci. Total Environ.*, 2013, 468–469.
10. Bhambri, R., Mehta, M., Dhobal, D. P. and Gupta, A. K., Glacier *Lake Inventory of Uttarakhand*, Wadia Institute of Himalayan Geology, 2015.
11. Randhawa, S. S., Sood, R. K., Rathore, B. P. and Kulkarni, A. V., Moraine-dammed lakes study in Chenab and Satluj river basins using IRS data. *J. Indian Soc. Remote Sensing*, 2005, **33**(2), 285–290.
12. Huggel, C., Kaab, A., Haeberli, W., Teysseire, P. and Paul, F., Remote sensing based assessment of hazards from glacier lake outbursts: a case study in the Swiss Alps. *Can. Geotech. J.*, 2002, **39**, 316–330.
13. Cuffey, K. M. and Paterson, W. S. B., *The Physics of Glaciers*, Butterworth-Heinemann, Oxford, 2010, 4th edn.
14. Gantayat, P., Kulkarni, A. V. and Srinivasan, J., Estimation of ice thickness using surface velocities and slope: case study at Gangotri Glacier, India. *J. Glaciol.*, 2014, **60**, 277–282.
15. Azam, M. F. *et al.*, From balance to imbalance: a shift in the dynamic behaviour of Chhota Shigri glacier, western Himalaya, India. *J. Glaciol.*, 2012, **58**, 315–324.

16. Farinotti, D., Huss, M., Bauder, A., Funk, M. and Truffer, M., A method to estimate ice volume and ice-thickness distribution of alpine glaciers. *J. Glaciol.*, 2009, **55**, 422–430.
17. Haeberli, W. and Hoelzole, M., Application of inventory data for estimating characteristics of regional climate-change effects on mountain glaciers: a pilot study with European Alps. *Ann. Glaciol.*, 1995, **21**, 206–212.
18. Hutchinson, M. F., ANUDEM version 5.3. User's guide, Australian National University Fenner School of Environment and Society, Canberra, Australia, 2011.
19. Linsbauer, A., Paul, F. and Haeberli, W., Modeling glacier thickness distribution and bed topography over entire mountain ranges with GlabTop: application of a fast and robust approach. *J. Geophys. Res.*, 2012, **117**, F03007.
20. Fischer, A., Calculation of glacier volume from sparse ice-thickness data, applied to Schaufelferner, Austria. *J. Glaciol.*, 2009, **55**, 453–460.
21. Lee, D., Storey, J., Choate, M. and Hayes, R., Four years of Landsat-7 on-orbit geometric calibration and performance. *IEEE Trans Geosci. Remote Sensing*, 2004, **42**, 2786–2795.
22. Leprince, S., Barbot, S., Ayoub, F. and Avouac, J. P., Automatic and precise orthorectification, coregistration, and subpixel correlation of satellite images, application to ground deformation measurements. *IEEE Trans. Geosci. Remote Sensing*, 2007, **45**, 1529–1558.
23. Fujita, K., Suzuki, R., Nuimura, T. and Sakai, A., Performance of ASTER and SRTM DEMs and their potential for assessing glacial lakes in the Lunand region, Bhutan Himalaya. *J. Glaciol.*, 2008, **54**, 220–228.
24. Nye, J. F., The flow of a glacier in a channel of rectangular, elliptic or parabolic cross-section. *J. Glaciol.*, 1965, **5**(41), 661–690.
25. Kulkarni, A. V., Dhar, S., Rathore, B. P., Raj, B. and Kalia, R., Recession of Samudra Tapu Glacier, Chandra River Basin, Himachal Pradesh. *J. Indian Soc. Remote Sensing*, 2006, **34**(2), 39–46.

Received 22 April 2016; revised accepted 14 June 2016

doi: 10.18520/cs/v111/i3/553-560

Characterization of hazardous solid waste (soot) accumulated in tailpipe of typical Indian share autos

Ravi Sahu, Prasenjit Adak and Suresh Pandian Elumalai*

Department of Environmental Science and Engineering, Indian School of Mines, Dhanbad 826 004, India

In this communication, accumulated soot from typical Indian share autos and buses has been characterized using FE-SEM coupled with EDS and FTIR spectroscopy for its toxicity level. Analysis reveals the size of spherical-shaped primary particles to be less than 40 nm, which agglomerate to form fractal-like structures. In share autos, average weight percentage of heavy metals such as Cr, Fe, Cu and Pt (except Zn) is higher than that in buses; trace elements include non-carbon elements. FTIR results suggest that share autos contaminate soil of paved and unpaved roadways to a greater extent and at a faster rate compared to buses.

Keywords: Heavy metals, road soil contamination, share auto, soot particles, vehicular solid waste.

IN developing countries, providing access to cheaper public road transport is a deciding factor for percentage share of vehicle types. Due to this reason share autos are now the leading public transport mode along with buses. This has resulted in exponential increase in their numbers over the past decade. Therefore, changes in the percentage share of vehicles plying on urban roads affect traffic and emission characteristics such as average traffic fleet speed, delay due to congestion and fuel consumption[1]. Share autos running with more than allotted capacity consume more fuel resulting in higher emissions[2–4]. Inadequate maintenance of vehicles enhances emission from them[5–9]. Besides, lack of controlling devices like catalytic converters and filters makes them even larger emitters of pollutants, especially soot particles. Therefore, it is important to study the chemical composition of soot particles emitted from share autos to understand their health and environmental impacts.

Several researchers have studied the chemical constituents of vehicular soot particles for their toxicity or carcinogenicity[10–13], and health impacts of emissions from diesel-driven vehicles on school-going children, adult commuters, drivers and passengers[14–17]. However, there is a limited number of publications discussing the composition of condensed soot particles which accumulate on the inner surface of the tailpipe of share autos. A small fraction of the volatile or semi-volatile content of the exhaust could subsequently undergo gas-to-particle conversion once it gets cooled to form the accumulated particles on the surface of the tailpipe[18,19]. Upon saturation, accumulated coarser soot particles are prone to desorption while subjected to external forces such as velocity and temperature of exhaust gas and mechanical disturbances caused due to vehicular speed. Owing to larger size and weight, desorbed soot containing polyaromatic hydrocarbons (PAHs) deposits around nearby areas, i.e. road soil[20]. These contaminated soils can pose a threat to human beings by virtue of re-suspension generated by moving vehicles.

The emission of soot particles is a result of incomplete combustion of fuel in the engines. Diesel particulate emissions consist of carbonaceous material, generally 75% elemental carbon (EC) known as 'soot' and 20% organic carbon (OC)[21]. The elemental fractions are generated from diesel fuel droplet during pyrolysis, whereas

*For correspondence. (e-mail: suresh.pe.ese@ismdhanbad.ac.in)